SOX9 drives WNT pathway activation in prostate cancer

Fen Ma,[1] Huihui Ye,[2] Housheng Hansen He,[3,4] Sean J. Gerrin,[2] Sen Chen,[1] Benjamin A. Tanenbaum,[1] Changmeng Cai,[1] Adam G. Sowalsky,[1] Lingfeng He,[1] Hongyun Wang,[1] Steven P. Balk,[1] and Xin Yuan[1]

[1]Division of Hematology/Oncology, Department of Medicine, and [2]Department of Pathology, Beth Israel Deaconess Medical Center, Harvard Medical School, Boston, Massachusetts, USA.

[3]Department of Medical Oncology and [4]Department of Biostatistics and Computational Biology, Dana-Farber Cancer Institute, Harvard Medical School, Boston, Massachusetts, USA.

The transcription factor SOX9 is critical for prostate development, and dysregulation of SOX9 is implicated in prostate cancer (PCa). However, the SOX9-dependent genes and pathways involved in both normal and neoplastic prostate epithelium are largely unknown. Here, we performed SOX9 ChIP sequencing analysis and transcriptome profiling of PCa cells and determined that SOX9 positively regulates multiple WNT pathway genes, including those encoding WNT receptors (frizzled [FZD] and lipoprotein receptor-related protein [LRP] family members) and the downstream β-catenin effector TCF4. Analyses of PCa xenografts and clinical samples both revealed an association between the expression of SOX9 and WNT pathway components in PCa. Finally, treatment of SOX9-expressing PCa cells with a WNT synthesis inhibitor (LGK974) reduced WNT pathway signaling in vitro and tumor growth in murine xenograft models. Together, our data indicate that SOX9 expression drives PCa by reactivating the WNT/β-catenin signaling that mediates ductal morphogenesis in fetal prostate and define a subgroup of patients who would benefit from WNT-targeted therapy.

Introduction

SOX9 belongs to the SOX (SRY-related HMG box) family of transcription factors and regulates many developmental processes. SOX9 mutations cause campomelic dysplasia, a disease that is characterized by extreme cartilage and bone malformation, multiple defects in other organs, and frequent XY sex reversal, demonstrating an important role in tissue development (1, 2). In adults, SOX9 is highly expressed by stem cells in the intestinal crypts where it is regulated by the canonical WNT/β-catenin/T cell factor (WNT/β-catenin/TCF) pathway (3). Recent work shows that SOX9 contributes to the maintenance of stem/progenitor cells in additional tissues, including liver, pancreas, and hair follicle (4–7). Dysregulated SOX9 expression has been implicated in the pathogenesis of cancers in multiple tissues, including colorectal, prostate, breast, pancreas, and lung tissues (8–13). However, the critical SOX9-regulated genes in most tissues and cancers remain to be established and are likely cell-type and developmental-stage specific.

SOX9 is also required for prostate development (10, 14). In fetal prostate, SOX9 is expressed by the epithelial cells invading the urogenital sinus mesenchyme during branch expansion (13, 15), and prostate-specific *Sox9* knockout causes a profound defect in prostate ductal morphogenesis (10, 14). In the adult prostate, SOX9 is expressed primarily by the basal cells, which are presumed to have roles in maintaining the luminal epithelium (12). Accumulating evidence strongly supports a role for SOX9 in prostate cancer (PCa) (11–13, 15, 16). Genome-wide association studies have mapped a PCa-associated 17q24.3 single nucleotide polymorphism to an enhancer of the *SOX9* gene (17). SOX9 is highly expressed in a subset of primary PCa, in which its expression is correlated with higher Gleason grades (11), and its expression is further increased in advanced castration-resistant PCa (12). In PCa xenograft models, increased SOX9 expression enhanced growth, invasion, and angiogenesis, while silencing of endogenous SOX9 markedly impaired tumor growth (13, 18). In mouse models, prostate-specific transgenic *Sox9* overexpression caused prostatic intraepithelial neoplasia and, in combination with a loss of one *Pten* allele, caused progression to invasive PCa (11, 18). Moreover, *Sox9* knockout prevented tumor development in two genetically engineered mouse models of PCa (TRAMP and Hi-Myc) (10).

TMPRSS2:ERG gene fusions, which occur in approximately 50% of PCa, place the transcription factor ERG under control of the *TMPRSS2* promoter, which is strongly regulated by the androgen receptor (AR), resulting in high-level androgen-stimulated expression of ERG (19). We recently reported an association between *TMPRSS2:ERG* gene fusion and increased SOX9 (18). At the molecular level, we found that ERG binds adjacent to a cryptic androgen-responsive element downstream of the *SOX9* gene, thereby opening this site for AR binding and androgen-stimulated expression of SOX9 (18). While ERG may similarly direct AR to additional genes (18, 20, 21), the profound effects of *SOX9* silencing on the growth and invasion of *TMPRSS2:ERG* fusion–positive VCaP PCa cells indicated that SOX9 is a critical effector of ERG in PCa. Overall these findings support a major role for SOX9 in PCa and suggest that its normal functions in prostate development may be reactivated in PCa to drive invasive growth. To test these hypotheses, we have used SOX9 ChIP sequencing (ChIP-seq) and transcriptome profiling to comprehensively identify the spectrum of SOX9-regulated genes and pathways in PCa.

Conflict of interest: The authors have declared that no conflict of interest exists.
Submitted: September 2, 2014; **Accepted:** February 9, 2016.
Reference information: *J Clin Invest*. 2016;126(5):1745–1758. doi:10.1172/JCI78815.

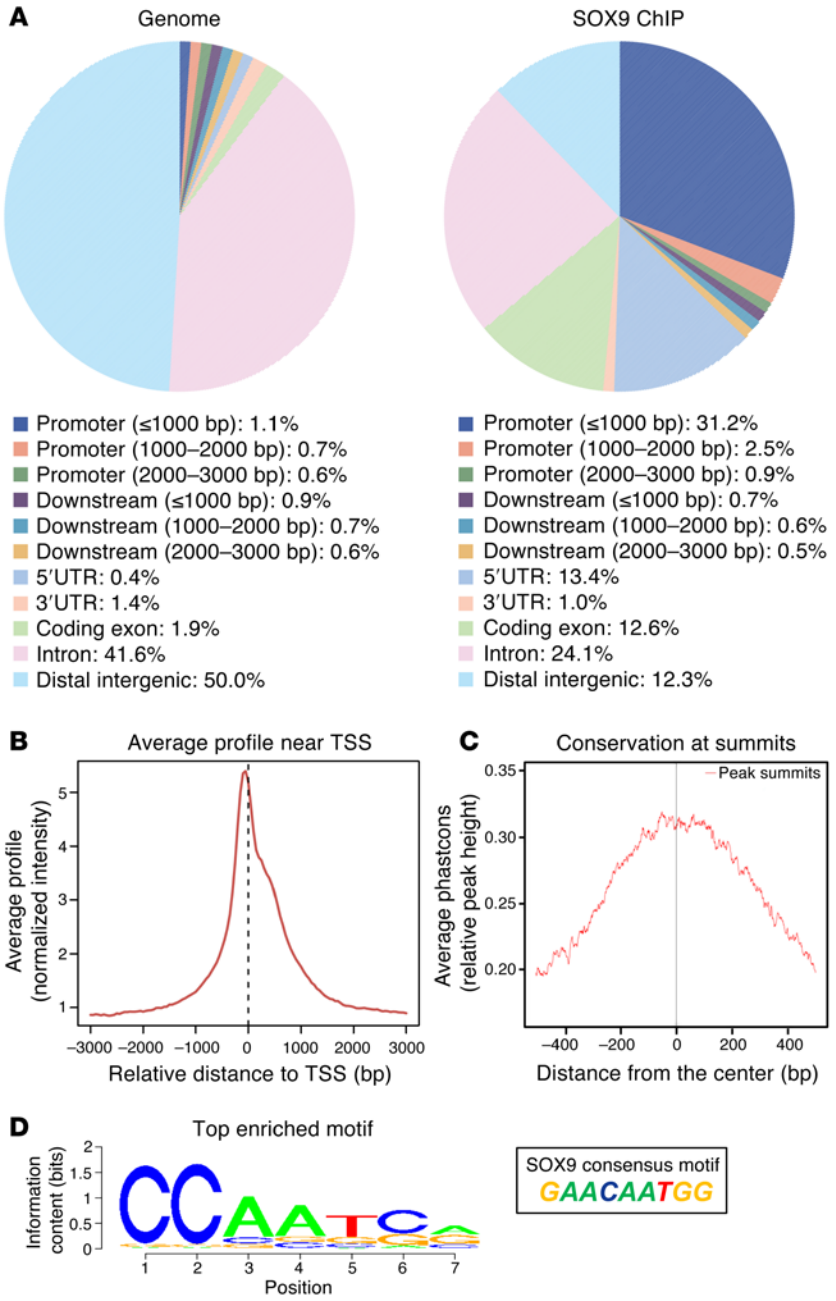

Figure 1. SOX9 chromatin binding in VCaP cells. (**A**) Pie charts demonstrating the distribution of features in genome (input control) and among SOX9-binding peaks. The listed genomic features include promoters (–1 kb to +1 kb; –2 kb to +2 kb; –3 kb to +3 kb of TSSs); downstream elements (–1 kb to +1 kb; –2 kb to +2 kb; –3 kb to +3 kb of transcription stop sites); gene body (5′UTR, 3′UTR, exons, and introns); and intergenic regions. (**B**) An average profile of SOX9-binding peaks near TSSs. (**C**) The conservation profile of SOX9-binding peaks. (**D**) The top consensus sequence motif compiled from SOX9-binding peaks within a 100-bp window centered on the binding summits. The consensus SOX9 motif based on oligonucleotide binding is also shown.

Results

SOX9-binding sites identified by ChIP-seq in TMPRSS2:ERG fusion–positive VCaP PCa cells. The *TMPRSS2:ERG* fusion–positive VCaP PCa cell line, which expresses high levels of endogenous SOX9 that critically support VCaP growth and invasion, was used as a model to identify SOX9 chromatin binding sites and SOX9-regulated genes (18). In pilot studies, we assessed two antibodies (referred to herein as Ab1 and Ab2) for ChIP of a well-characterized SOX9-binding site in the *Col2a1* gene (22). As shown in Supplemental Figure 1A (supplemental material available online with this article; doi:10.1172/JCI78815DS1), ChIP effectively brought down this SOX9 site, with Ab1 being more effective. We then carried out SOX9 ChIP-seq in VCaP cells using these two anti-SOX9 antibodies in parallel. Peak calling by the model-based analysis for ChIP-seq (MACS) algorithm revealed 7,547 sites with the SOX9 Ab1 (at a false discovery rate of 5%). Many fewer sites and lower peak intensities were observed with SOX9 Ab2, consistent with its lower efficiency on the control *Col2a1* gene, and these sites overlapped the higher peak intensity sites identified by the SOX9 Ab1 (data not shown). Therefore, the subsequent analyses were based on the SOX9 Ab1 ChIP-seq data.

In support of the ChIP-seq results, we could identify peaks associated with several genes previously found to be SOX9 regulated, including *COMP*, *Col11a2*, *Col2a1*, and *Col4a2* (Supplemental Figure 1, B and C). Compared with the distribution of features in the human genome, SOX9-binding sites were greatly enriched in the promoter regions, with 31.2% of sites within 1 Kb upstream of transcription start sites (TSSs) and 13.4% in 5′UTRs (Figure 1A). The peak intensity profile of these sites flanking the TSS is shown in Figure 1B. A conservation analysis showed that sequences in and flanking the SOX9-binding sites are evolutionarily conserved, supporting their functional significance (Figure 1C). Sequence motif searches of the SOX9-binding peaks showed the greatest enrichment for the sequence CCAATC, which is divergent but related to the consensus SOX9 motif (AACAAT) that was identified previously by random oligonucleotide screening (ref. 23 and Figure 1D). Recent SOX9 ChIP studies in other cell types have similarly found substantial divergence from the SOX9 consensus motif (24–26).

To determine whether SOX9 may be interacting with other transcription factors in a subset of SOX9-binding sites, we scanned flanking sequences for transcription factor motifs. This revealed enrichment for motifs recognized by transcription factors, including AP2, LRF, ETF, WT1, and E2F (Supplemental Figure 1D and Supplemental Table 1). Interestingly, LRF (also known as ZBTB7A) was reported to interact with SOX9 and repress SOX9-mediated stimulation of a long noncoding RNA that prevents cellular senescence in mouse prostate cells (27). Finally, to determine whether specific pathways may be regulated by these transcription factors

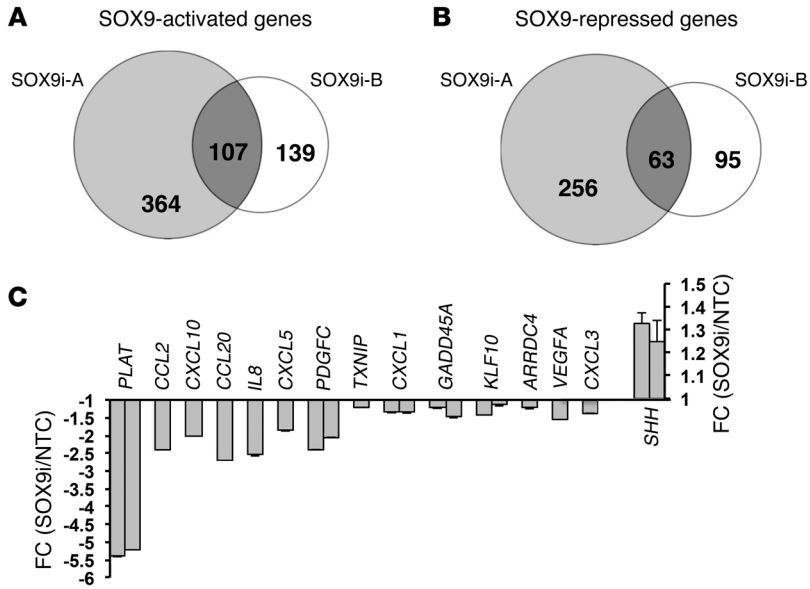

Figure 2. SOX9-regulated transcriptome in VCaP cells. (**A**) An expression profile of genes reduced after SOX9 knockdown by SOX9i-A or SOX9i-B transfections (SOX9-activated genes). (**B**) Profile of genes increased after SOX9 knockdown (SOX9-suppressed genes). (**C**) qRT-PCR measurement of the relative fold of changes (FC) in mRNA levels of SOX9-responsive genes after SOX9 knockdown compared with those of nontargeting siRNA controls (NTC). Each bar represents the result from one primer set, with some genes being examined with 2 independent primer sets (see the Supplemental Methods for primer sequences). Error bars represent SD.

in conjunction with SOX9, we used Ingenuity pathway analysis to analyze the genes associated with these sites for each transcription factor but did not find significant enrichment for any pathway gene sets (data not shown).

SOX9-regulated transcriptome in VCaP cells. We next identified two independent SOX9 siRNAs (SOX9i-A and -B) that effectively decreased SOX9 levels in VCaP cells (Supplemental Figure 2). These siRNAs were then used to transiently decrease SOX9 expression in VCaP cells, and RNA from these cells or control cells treated with nontargeting siRNAs was harvested and analyzed on Affymetrix GeneChip Human Genome U133 Plus 2.0 Arrays. SOX9i-A decreased the expression of 471 genes by >1.5-fold. SOX9i-B decreased the expression of 246 genes by >2.0-fold (as SOX9i-B was more potent in repressing *SOX9* gene expression, we used a more stringent cutoff). There were 107 decreased genes that overlapped between these two siRNAs (SOX9-activated genes, Figure 2A). Similarly, the expression of 319 and 158 genes was increased by SOX9i-A and -B, respectively, with an overlap of 63 genes (SOX9-repressed genes, Figure 2B). Based on these data, the top-ranked SOX9-activated and -repressed genes are listed in Supplemental Tables 2 and 3. Using quantitative RT-PCR (qRT-PCR) in VCaP cells, we confirmed that expression of a series of these genes was activated by SOX9 (decreased by SOX9 siRNA) and that *SHH* expression was repressed by SOX9 (increased by SOX9 siRNA) (Figure 2C).

Gene set enrichment analysis (GSEA) was then performed to identify pathways that may be regulated by SOX9. This identified a number of pathways that have been implicated in PCa, including the hedgehog, MAPK, NOTCH, JAK/STAT, cytokine, chemokine, and WNT signaling pathways (Supplemental Table 4). To assess whether these pathways may be related to SOX9 in vivo, we carried out GSEA to identify pathways associated with increased *SOX9* mRNA in The Cancer Genome Atlas (TCGA) and Memorial Sloan Kettering Cancer Center (MSKCC) (28) primary PCa gene expression data sets. With the exception of hedgehog, each of the above pathways was associated with increased SOX9 in both data sets (Supplemental Tables 5 and 6). NOTCH signaling showed the strongest correlation in both the TCGA and MSKCC data sets, which may in part reflect the reported NOTCH regulation of SOX9 expression (29–31). The correlation with MAPK signaling may also reflect the reported SOX9 induction through activation of receptor tyrosine kinases, including FGFRs and MET (16, 32).

SOX9 regulation of WNT signaling. We focused on the relationship between SOX9 and the WNT signaling pathway, based on the following observations. Previous studies have shown that SOX9 expression may be increased downstream of WNT/β-catenin signaling. In particular, SOX9 expression in colonic crypts is stimulated by β-catenin/TCF4 (33), and we reported previously that SOX9 expression could be stimulated by WNT signaling in PCa cells (12). Significantly, SOX9 is expressed by urogenital sinus epithelium in mouse and human fetal prostate and is critical for prostate ductal morphogenesis (10, 13, 14). This developmental process is also dependent on canonical WNT/β-catenin signaling (34), but the relationship between SOX9 and WNT signaling in prostate development and, in particular, whether SOX9 is upstream or downstream of WNT signaling in prostate, has not been established. Interestingly, recent studies have linked ERG in *TMPRSS2:ERG* fusion–positive PCa to WNT signaling (35, 36), which may be a direct effect of ERG or may be in part mediated indirectly through ERG-induced SOX9 (18). Finally, we recently reported an association between SOX9 expression and the WNT/β-catenin pathway in triple-negative breast cancer and found that SOX9 could increase the expression of TCF4 and a WNT coreceptor, lipoprotein receptor-related protein 6 [LRP6], in breast cancer cells (37). Together, these results supported a link between SOX9 and WNT signaling.

The WNT pathway GSEA for control versus SOX9-depleted VCaP cells is shown in Figure 3A. The most highly regulated WNT pathway gene was the WNT receptor *FZD7*, with additional frizzled [FZD] family receptors also being increased (*FZD6* and *FZD9*) or decreased (*FZD3*, *FZD8*, and *FZD5*) by SOX9 (Figure 3B). *LRP5*, a coreceptor with FZD family receptors for WNTs, was also increased. Downstream of WNT receptors, expression of *DVL1* and *TCF4* (also known as *TCF7L2*) was increased, as was

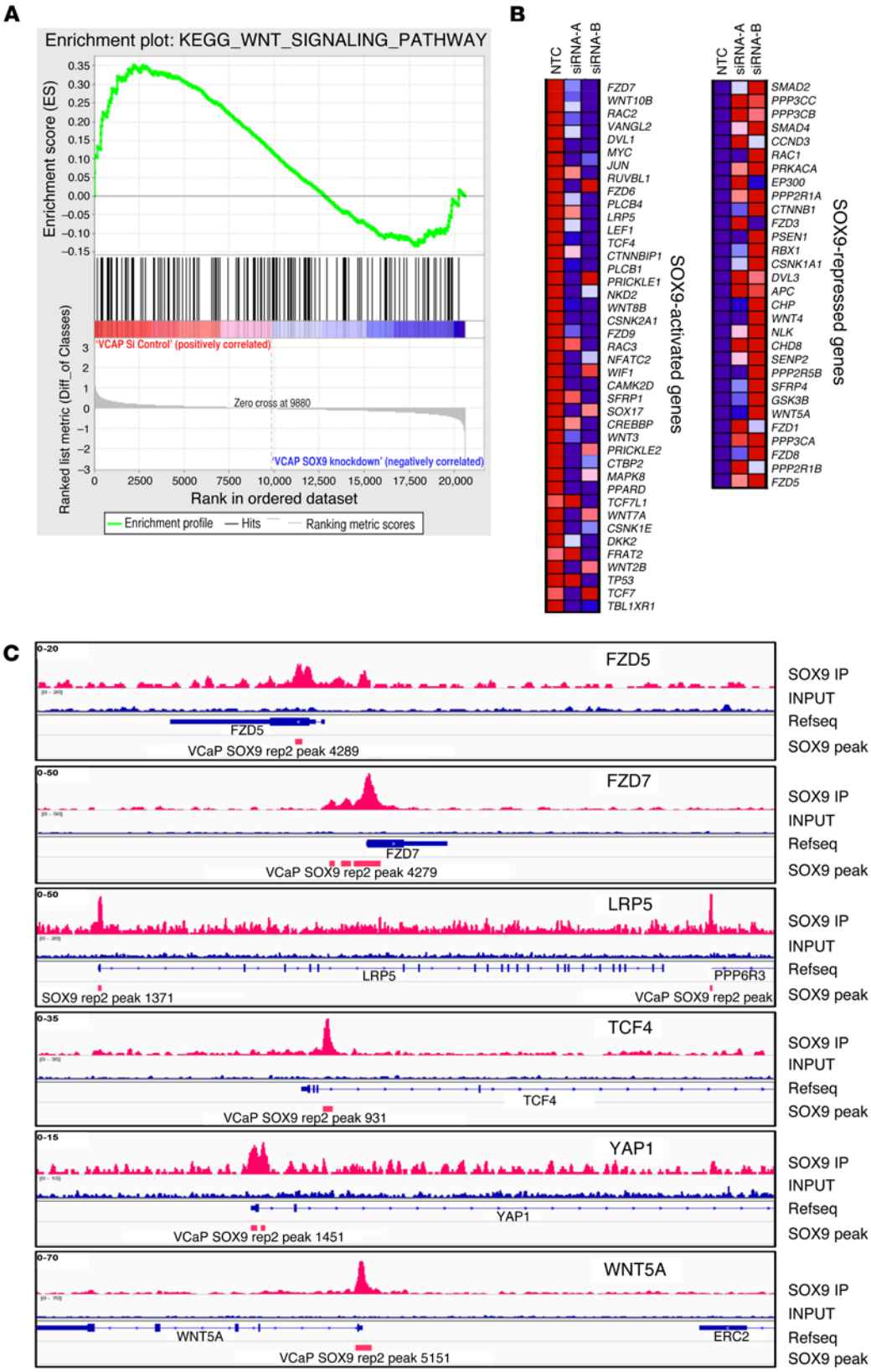

Figure 3. SOX9 regulation of multiple WNT signaling components in VCaP cells. (**A**) GSEA of SOX9-responsive genes shows enrichment of the WNT signaling pathway in VCaP cells. Normalized enrichment score (NES) = 1.00. (**B**) Heat maps comparing the expression of WNT component genes after transfection with nontargeting control (NTC), SOX9i-A, or SOX9i-B. (**C**) Binding profiles and peak calling records of representative WNT component genes in SOX9 ChIP-seq analysis (within 100 kb upstream and downstream of each gene). Significant peaks ($P < 1 \times 10^{-15}$) are noted in the SOX9 PEAK row.

expression of the β-catenin/TCF4-regulated *MYC* and *LEF1* genes (Figure 3B). Significantly, Yes-associated protein 1 (*YAP1*) was also increased by SOX9 (Supplemental Table 7). YAP1 is a transcriptional coactivator that is negatively regulated by the Hippo pathway (38). However, it was recently found to bind β-catenin, with the β-catenin/YAP1 complex regulating genes involved in cell growth/survival, thereby opposing the growth inhibitory Hippo pathway (39). Finally, several WNTs were increased by SOX9,

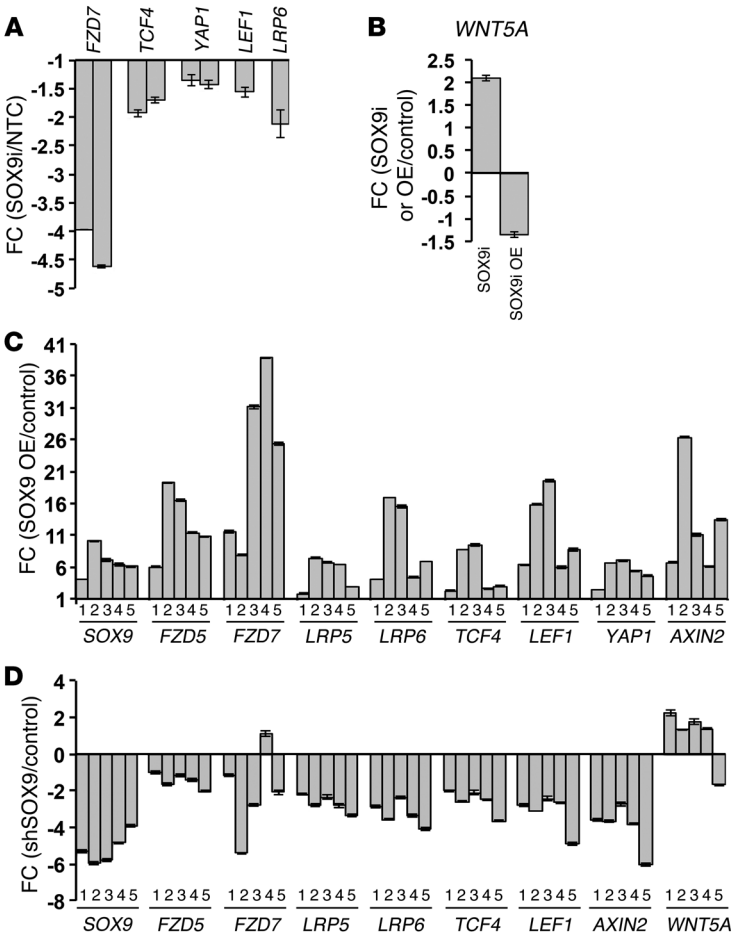

Figure 4. Validation of SOX9-regulated expression of WNT pathways genes and activity in vitro and in vivo. (**A**) Levels of WNT components were measured by qRT-PCR in VCaP cells transfected with SOX9i or control siRNA. The relative mRNA levels are shown as fold change between SOX9i and nontargeting control (NTC). For each gene, one bar represents one primer set (some genes were assessed with two independent primer sets; see the Supplemental Methods for primer sequences). (**B**) Levels of WNT5A were measured by qRT-PCR in VCaP cells transfected with siRNA (SOX9i) or in a stable VCaP cell line overexpressing SOX9 (SOX9-OE). The results are presented as the fold change compared with their corresponding controls. (**C**) Levels of *SOX9* and WNT components were measured by qRT-PCR in 5 LNCaP SOX9-OE xenografts derived from a LNCaP cell line with inducible SOX9 overexpression (SOX9-OE, $n = 5$). The relative mRNA levels are shown as fold change between SOX9-OE and uninduced control. The numbers 1–5 indicate results from 5 independent xenografts. (**D**) Levels of *SOX9* and WNT components were measured by qRT-PCR in 5 CWR22Rv1 xenografts derived from a stable SOX9 shRNA expressing cell line (shSOX9, $n = 5$). The relative mRNA levels are shown as fold change between shSOX9 and control. All error bars represent SD.

while *WNT5A* was strongly repressed (Figure 3B). In contrast to other WNTs, WNT5A is a ligand for the ROR1 and ROR2 receptor tyrosine kinases, and the noncanonical signaling through this pathway generally opposes canonical WNT/β-catenin signaling (40–42). A schematic demonstrating the broad regulation of WNT components by SOX9 is shown in Supplemental Figure 3.

To assess whether SOX9 may be directly regulating these WNT pathway genes, we examined the SOX9 ChIP-seq data. Significantly, the majority of the SOX9-regulated WNT pathway genes had associated SOX9-binding sites within 20 Kb of their TSSs (83% versus ~33% genome wide) (Figure 3C, Supplemental Figure 4, and Supplemental Table 7). Among these genes showing SOX9-binding peaks, there was a weak but significant ($P < 1 \times 10^{-15}$) peak associated with the *YAP1* gene, indicating that it may be directly regulated by SOX9.

Validation of SOX9 regulation of the WNT pathway in PCa cells in vitro and in vivo. Using qRT-PCR, we next confirmed the effects of SOX9 siRNA in VCaP cells on a series of WNT pathway genes, including *FZD7*, *TCF4*, *LRP6*, and *YAP1* (with *FZD7* being most affected and *YAP1* being least affected, at ~1.3-fold decreased) (Figure 4A). Moreover, we confirmed that expression of the β-catenin/TCF4-regulated *LEF1* gene, which may also be directly regulated by SOX9 (Supplemental Table 7), was decreased by SOX9 RNAi. Finally, we confirmed the SOX9-negative regulation of *WNT5A* by showing that SOX9 siRNA increased and SOX9 overexpression reduced *WNT5A* expression (Figure 4B).

We next examined PCa xenografts to further assess whether SOX9 was regulating WNT pathway genes in vivo. We had previously shown that SOX9 overexpression in LNCaP cell subcutaneous xenografts increases initial tumor growth and invasion (13). Therefore, we extracted RNA from a series of these xenografts generated with LNCaP cells overexpressing SOX9 (SOX9-OE xenografts) and control parental LNCaP xenografts and assessed them for WNT pathway gene expression by qRT-PCR. As expected, *SOX9* expression in all 5 LNCaP SOX9-OE xenografts examined was increased relative to control (Figure 4C). Significantly, expression of SOX9-stimulated WNT pathway genes (*FZD5*, *FZD7*, *LRP5*, *LRP6*, *TCF4*, and *YAP1*) also was increased in the LNCaP SOX9-OE xenografts, as was expression of *LEF1* and *AXIN2* (Figure 4C). Interestingly, WNT5A was increased in the LNCaP SOX9-OE xenografts, indicating that it is activated by SOX9 in this model in contrast to its being suppressed in the VCaP cell line (data not shown). The basis for this difference is not yet clear. We similarly examined a series of xenografts derived from an independently derived LNCaP SOX9-OE cell line and also found an increase in each of these WNT pathway genes (Supplemental Figure 5).

We showed previously that SOX9 depletion markedly impaired or abrogated the ability to establish VCaP xenografts (18), so we could not use VCaP xenografts to examine the in vivo effects of SOX9 depletion on WNT pathway genes. Therefore, we next examined CWR22Rv1 xenografts. Although these CWR22Rv1 cells do not have the *TMPRSS2:ERG* fusion, we showed previ-

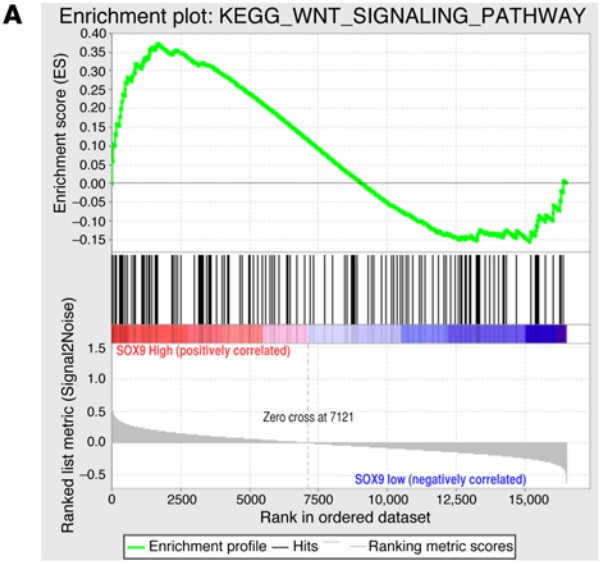
A
Enrichment plot: KEGG_WNT_SIGNALING_PATHWAY
Enrichment score (ES)
SOX9 High (positively correlated)
Zero cross at 7121
SOX9 low (negatively correlated)
Ranked list metric (Signal2Noise)
Rank in ordered dataset
Enrichment profile — Hits — Ranking metric scores

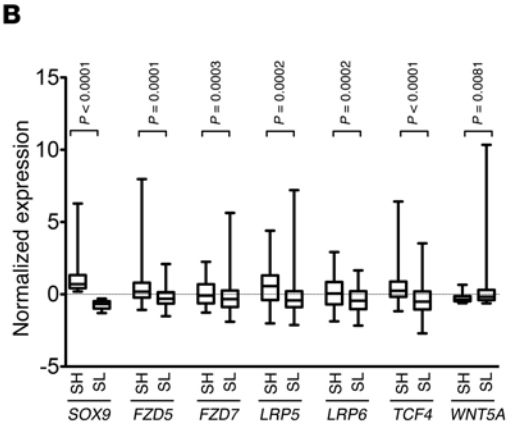
B
Normalized expression
P < 0.0001
P = 0.0001
P = 0.0003
P = 0.0002
P = 0.0002
P < 0.0001
P = 0.0081
SH SL
SOX9 FZD5 FZD7 LRP5 LRP6 TCF4 WNT5A

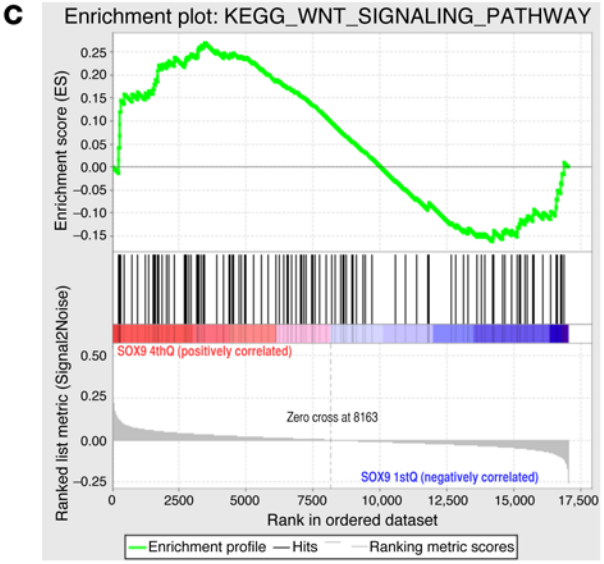
C
Enrichment plot: KEGG_WNT_SIGNALING_PATHWAY
Enrichment score (ES)
SOX9 4thQ (positively correlated)
Zero cross at 8163
SOX9 1stQ (negatively correlated)
Ranked list metric (Signal2Noise)
Rank in ordered dataset
Enrichment profile — Hits — Ranking metric scores

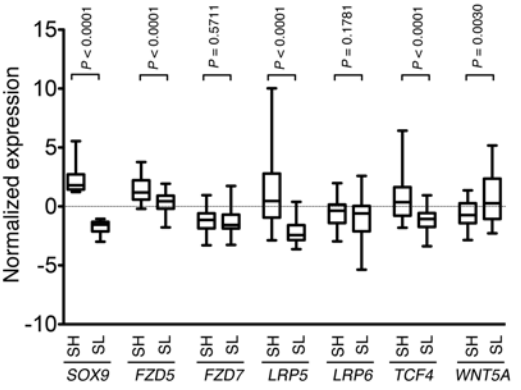
D
Normalized expression
P < 0.0001
P < 0.0001
P = 0.5711
P < 0.0001
P = 0.1781
P < 0.0001
P = 0.0030
SH SL
SOX9 FZD5 FZD7 LRP5 LRP6 TCF4 WNT5A

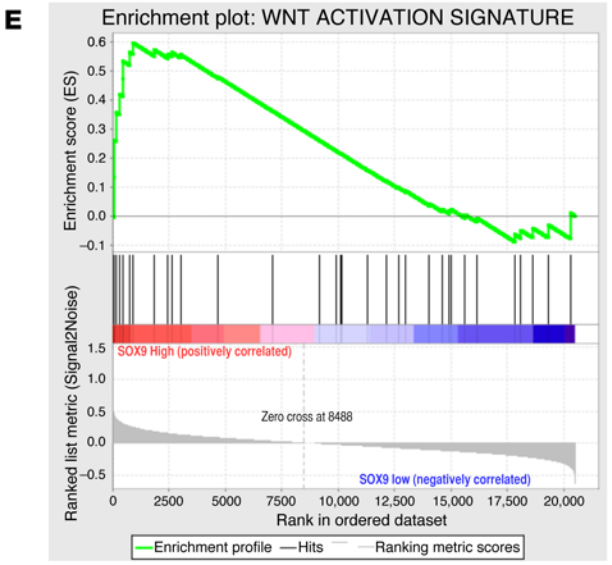
E
Enrichment plot: WNT ACTIVATION SIGNATURE
Enrichment score (ES)
SOX9 High (positively correlated)
Zero cross at 8488
SOX9 low (negatively correlated)
Ranked list metric (Signal2Noise)
Rank in ordered dataset
Enrichment profile — Hits — Ranking metric scores

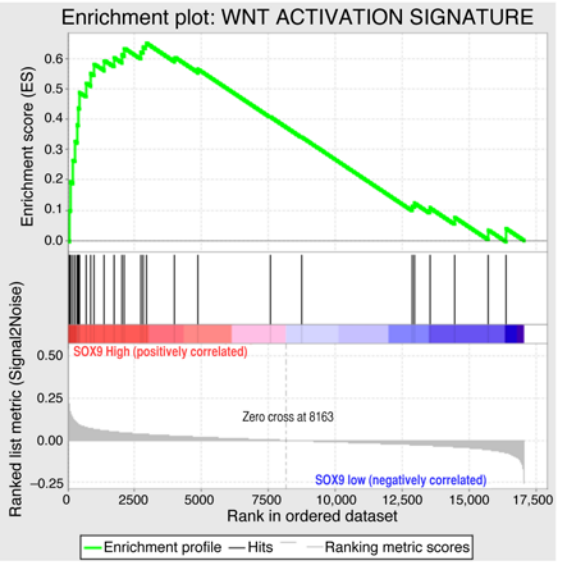
F
Enrichment plot: WNT ACTIVATION SIGNATURE
Enrichment score (ES)
SOX9 High (positively correlated)
Zero cross at 8163
SOX9 low (negatively correlated)
Ranked list metric (Signal2Noise)
Rank in ordered dataset
Enrichment profile — Hits — Ranking metric scores

Figure 5. SOX9-associated WNT pathway enrichment and expression of WNT signaling components in clinical PCa data sets. (**A**) GSEA of the WNT signaling pathway comparing SOX9 high and SOX9 low samples in the TCGA PCa data set. NES = 1.11. (**B**) The box plot demonstrates the differential expression of various WNT pathway components between the SOX9 high (SH, *n* = 60) and SOX9 low groups (SL, *n* = 85) from a cohort of 195 patients in the TCGA data set. Unpaired *t* test was used. (**C**) GSEA of the WNT signaling pathway in an MSKCC PCa data set comparing SOX9 high and SOX9 low samples. NES = 1.05. (**D**) The box plot demonstrates the differential expression of WNT components in the SOX9 high (*n* = 36) and SOX9 low groups (*n* = 28) from a cohort of 131 patients in the MSKCC data set. Unpaired *t* test was used. (**B** and **D**) In box-and-whisker plots, horizontal bars indicate the medians, boxes indicate 25th to 75th percentiles, and whiskers indicate 10th and 90th percentiles. (**E** and **F**) Enrichment profiles of the WNT activation signature adapted from ref. 43 comparing patients with high versus low levels of SOX9 expression in the TCGA (**E**) or MSKCC (**F**) data sets. The NES are 1.28 and 1.60, respectively.

ously that they express substantial levels of SOX9 and that SOX9 depletion slows (but does not prevent) their growth as xenografts (13). In a series of CWR22Rv1-shSOX9 xenografts, we found consistent decreases in *FZD5*, *FZD7*, *LRP5*, *LRP6*, *TCF4*, *LEF1*, and *AXIN2* and increases in *WNT5A* compared with that in control CWR22Rv1 xenografts (Figure 4D). Together, these in vitro and in vivo data indicate that there is WNT pathway activation in PCa and that SOX9 is one of the drivers of this activation through regulation of key WNT pathway components.

Correlation between SOX9 and WNT pathway activation in transgenic mouse models and in clinical samples. GSEA revealed that the WNT signaling pathway was enriched in PCa with high expression of SOX9 (SOX9 high) compared with that in PCa with low expression of SOX9 (SOX9 low) in the TCGA and MSKCC clinical data sets, indicating an in vivo and clinically relevant association between SOX9 and the WNT pathway (Figure 5, A and C). Similar to the results in VCaP cells, expression of *FZD5*, *FZD7*, *LRP5*, *LRP6*, and *TCF4* was positively associated, while *WNT5A* was negatively associated, with SOX9 levels in both clinical data sets (Figure 5, B and D). The corresponding heatmaps are shown in Supplemental Figure 6.

Significantly, the WNT pathway gene set used for this analysis was derived from studies across a wide range of cell types and is not specifically a signature of WNT pathway activation. Therefore, we also examined a gene set indicative of WNT pathway activation derived from colon cancer cells, which was also validated in breast cancer (43). GSEA with this WNT pathway activation gene set showed a strong correlation with SOX9 expression in both the TCGA and MSKCC data sets (SOX9 is in this gene set but was removed for this analysis to avoid artifactual inflation of the enrichment score) (Figure 5, E and F). The corresponding heatmaps are shown in Supplemental Figure 7.

It should be noted that *FZD5* was the FZD family WNT receptor most associated with increased SOX9 in these data sets, while *FZD5* was repressed by SOX9 in VCaP cells. Also, a previous study found an association between *TMPRSS2:ERG* fusion and increased *FZD4* (35). These findings, in conjunction with SOX9 chromatin binding sites associated with multiple FZD family genes, including *FZD5* and *FZD7* (Supplemental Table 7), indicate that SOX9 contributes to the regulation of multiple FZD family receptors and that SOX9 cooperation with additional transcriptional factors likely determines the magnitude and direction of regulation for particular FZD family receptors. The extent to which *LRP5* and *LRP6* are regulated by SOX9 may similarly be modulated.

To independently validate these findings, we next assessed SOX9-regulated WNT pathway activity in our previously reported transgenic mouse PCa models, in which prostate-specific SOX9 overexpression increased tumor formation and invasion in a *Pten*$^{+/-}$ background (18). We found that WNT activity (as indicated by *Axin2* in situ hybridization [ISH]) and SOX9 protein levels were modestly increased in prostatic intraepithelial neoplasia lesions of the *Pten*$^{+/-}$ mouse prostate (Figure 6A). However, *Axin2* levels were further increased (together with the markedly increased SOX9) in the prostatic intraepithelial neoplasia lesions in the *Pten*$^{+/-}$ *Sox9* mice.

We then examined an independent series of PCa clinical samples for SOX9-associated WNT activity. Figure 6B shows SOX9 immunohistochemistry (IHC) in representative primary PCa specimens with high or low SOX9 expression, which then were examined by ISH to assess the expression of *AXIN2* (a marker of WNT/β-catenin pathway activation) and of *FZD7* and *FZD5* (the WNT receptor most correlated with SOX9 in the clinical gene expression data sets). The results for this series of cases were then quantified, which showed that SOX9 expression was positively associated with increased WNT pathway signaling (Figure 6C). Finally, we found increased YAP1 by IHC in a subset of PCa expressing high levels of SOX9 (Figure 6D), although YAP1 was not consistently increased in SOX9 high tumors (possibly reflecting control of its expression by the Hippo pathway). Interestingly, YAP1 was coexpressed with SOX9 in the basal cells of normal prostate glands, suggesting roles for these proteins in regulating growth of the normal prostate epithelium (Figure 6D).

SOX9-driven WNT activity in PCa cells in vitro. Significantly, SOX9 depletion by siRNA caused a decrease in the levels of active (unphosphorylated) β-catenin (ABC) and WNT pathway–regulated MYC, cyclin D1, and LEF1 proteins, although the latter appeared to also be directly regulated by SOX9 (AXIN2 protein was not clearly detectable by immunoblotting in these cells; data not shown) (Figure 7A). This result, in conjunction with the SOX9 regulation of multiple WNT receptors and transducers, suggested that VCaP cells might have significant basal WNT pathway activity. To assess for basal endogenous WNT pathway activity, we treated VCaP cells with a potent small-molecule inhibitor (LGK974) of the enzyme porcupine, which is required for WNT palmitoylation, release, and receptor activation (44). At low nanomolar concentrations, LGK974 caused a decrease in phosphorylation of the WNT coreceptor LRP6, consistent with blockage of WNT receptor activation by endogenous WNT (Figure 7B). This was also associated with a decrease in levels of ABC (Figure 7B). Significantly, these decreases in ABC were most pronounced at higher concentrations of LGK974, which may reflect pathway activation by even very low levels of WNT (although some off-target effects of LGK974 cannot be excluded). Finally, treatment with the WNT coreceptor antagonist Dickkopf-related protein 1 (DKK1) similarly suppressed basal LRP6 phosphorylation, further indicating that the pathway is being stimulated by endogenous WNT (Supplemental Figure 8).

We next treated VCaP cells with LGK974 at concentrations that strongly suppressed ABC levels (0.5–1.0 μM) and assessed effects

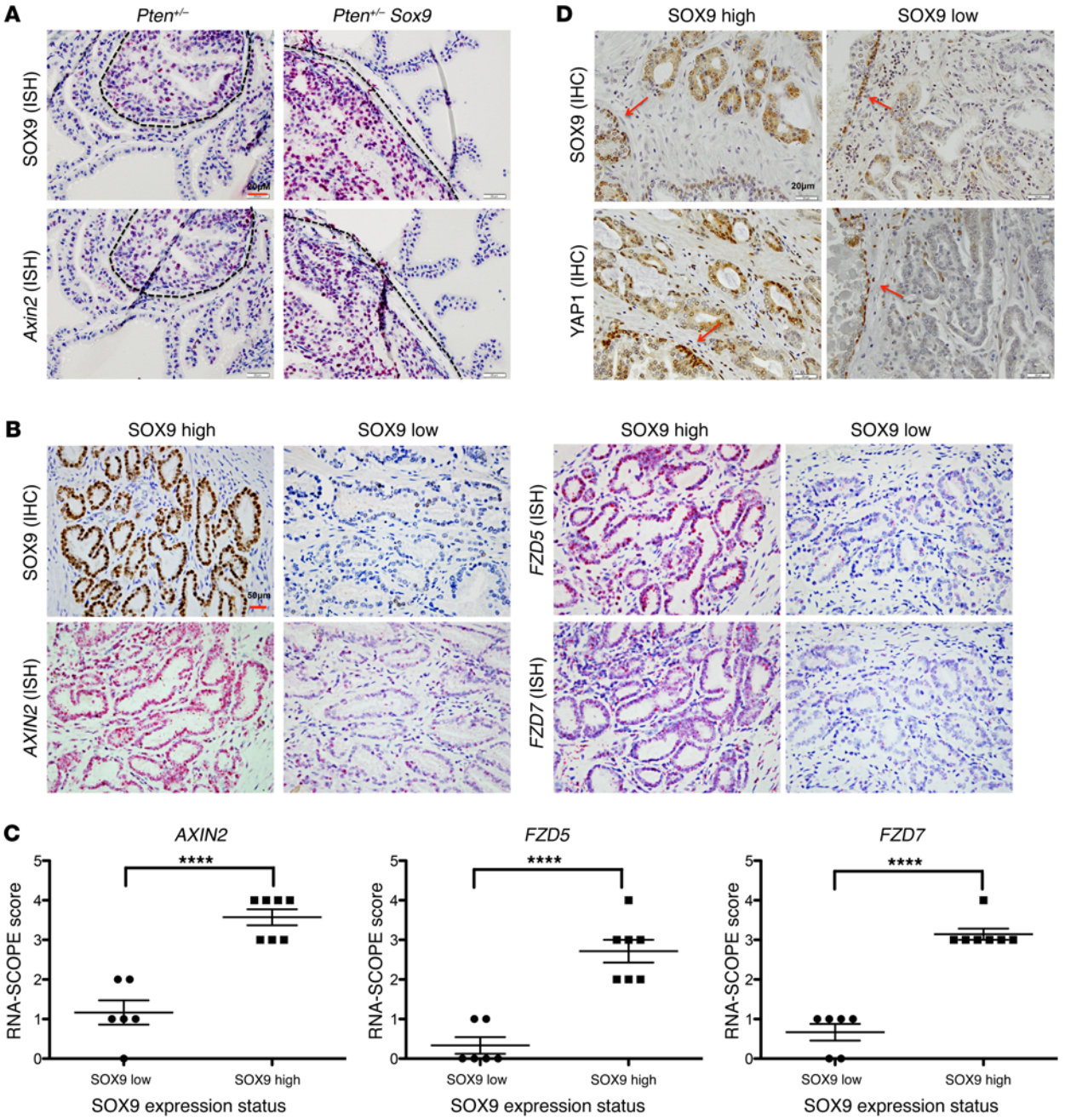

Figure 6. SOX9 correlates with WNT activity and expression of WNT components in transgenic mouse models and in primary PCa. (**A**) *Sox9* and *Axin2* expression was assessed by ISH in the prostates of *Pten*$^{+/-}$ or *Pten*$^{+/-}$ *Sox9* transgenic mice. The prostatic intraepithelial neoplasia lesions are encircled by dotted lines. Scale bar: 20 μm. (**B**) Representative illustration of levels of *AXIN2* (WNT activity) and *FZD5* or *FZD7* (SOX9-regulated WNT components) in SOX9 high or low primary PCa clinical samples. SOX9 was measured by IHC, while *AXIN2*, *FZD5*, and *FZD7* were examined by ISH. Scale bar: 50 μM. (**C**) Scatter plots demonstrate the differential WNT activity (reflected by *AXIN2* expression) or the expression of WNT receptors between SOX9 high (n = 7) and SOX9 low (n = 6) samples. SOX9 high was defined as >50% positive staining by IHC, and SOX9 low was defined as 0% and 5% positive staining. *AXIN2*, *FZD5*, and *FZD7* mRNA levels were measured by ISH (RNASCOPE). Error bars represent SEM. Data were analyzed by unpaired t test. ****$P < 0.0001$. (**D**) YAP1 protein levels measured by IHC between SOX9 high and SOX9 low PCa. Arrows indicate a positive stain of SOX9 or YAP1 in the basal cells of normal glands. Scale bar: 20 μM.

on WNT pathway activity. Consistent with suppression of WNT signaling, we found marked decreases in the WNT/β-catenin–regulated proteins MYC, cyclin D1, and LEF1 (Figure 7C). SOX9 was similarly decreased, a finding consistent with SOX9 expression being stimulated by β-catenin/TCF4 (12). We also treated VCaP cells with PKF118-310, an agent that disrupts β-catenin binding to TCF4 (45), and similarly observed decreased expression of these WNT/β-catenin–regulated genes (Figure 7C). Interestingly, ABC was also decreased after PKF118-310 treatment, which we presume was due to the displacement of unphosphorylated β-catenin from TCF4 or possibly other proteins and its subsequent phosphorylation and degradation (12, 44–46).

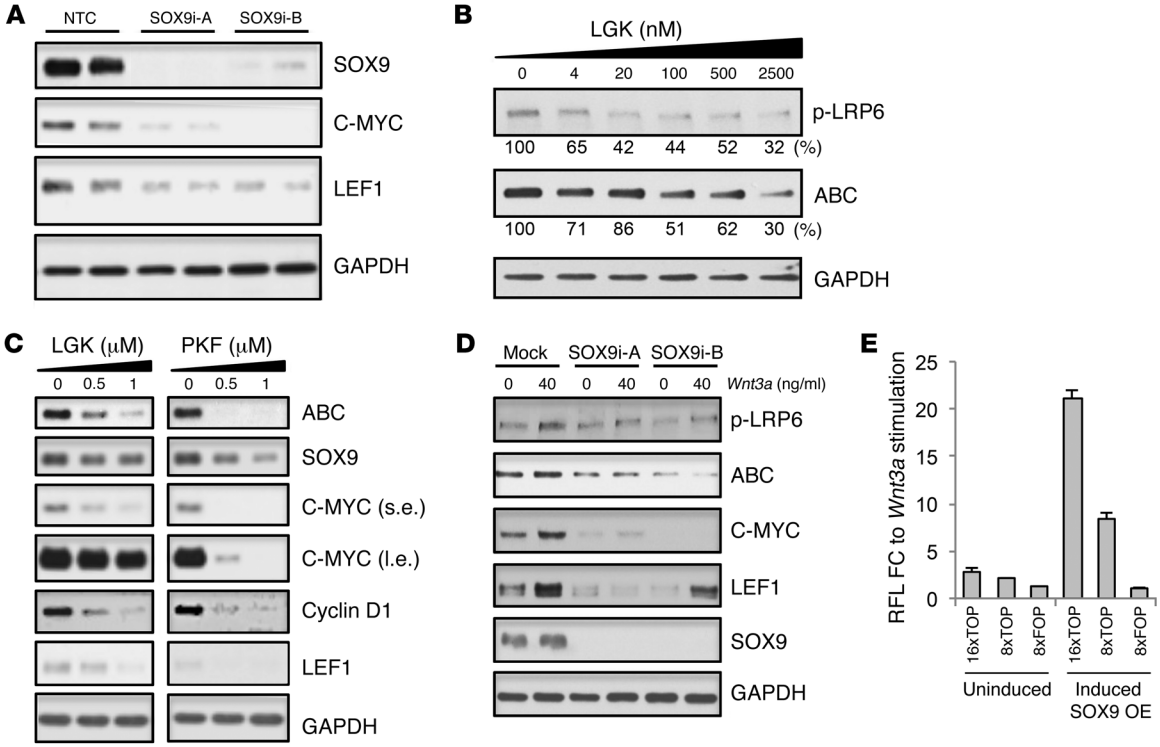

Figure 7. SOX9-dependent and autocrine WNT activation in VCaP cells. (**A**) VCaP cells were transfected with SOX9-targeted (SOX9i) or control (nontargeting control) siRNA. Cells were lysed and immunoblotted at 72 hours after transfection. (**B**) VCaP cells were treated with increasing concentrations of LGK974 (LGK) and were then lysed at 19 hours after treatment and immunoblotted. Band intensities were quantified using ImageJ software and normalized relative to the quantity of their respective GAPDH bands and are expressed as percentages of the first lane. (**C**) VCaP cells were treated with two independent WNT inhibitors: LGK974 or PKF118-310 (PKF). Cells were lysed at 19 hours after treatment and immunoblotted. The same untreated control sample is shown for both the LGK974 and PKF118-310 treatments. s.e., shorter exposure; l.e., longer exposure. (**D**) VCaP cells were mock transfected or transfected with SOX9-targeted siRNA (SOX9i). These cells were treated with either 0 or 40 ng/ml WNT3A during the last 6 hours before being lysed at 72 hours after transfection. (**E**) LNCaP cells with or without doxycycline-induced SOX9 overexpression (SOX9-OE) were transfected with 16× TOP-flash, 8× TOP-flash, or 8× FOP-flash plasmids, respectively, which was accompanied by pRL-CMV plasmid as a normalization control. The cells were lysed and measured for luciferase activity at 28 hours after transfection, and WNT3A (0 or 40 ng/ml) was added during the last 10 hours. The RFL activity of each transfection was calculated by normalizing the firefly luciferase activity against the reference renilla luciferase activity. The fold changes of the WNT3A stimulated and unstimulated basal RFL for each reporter are plotted. Error bars represent SD. Results in **A**–**D** are representative of 3 independent experiments each, and results in **E** are representative of 2 independent experiments, with triplicate biological replicates in each experiment.

Basal WNT pathway activity in VCaP cells could be increased by treatment with exogenous WNT3A, as indicated by increased p-LRP6, ABC, MYC, LEF1, and SOX9 (Figure 7D). Significantly, SOX9 silencing with siRNA reduced or abrogated these responses to WNT3A, consistent with the SOX9 regulation of WNT receptors and downstream transducers. To further directly assess whether SOX9 is sufficient in regulating the responses to WNT stimulation, we examined LNCaP cells with doxycycline-inducible SOX9. Cells were transfected with β-catenin/TCF4 or control-regulated firefly luciferase reporter genes (TOPflash or FOPflash, respectively), and SOX9 expression (SOX9-OE) was induced at the time of plating by addition of doxycycline (induced) or vehicle (uninduced). TOPflash, but not FOPflash, luciferase activity was markedly stimulated by WNT3A in the doxycycline-induced cells, while the TOPflash activity was only minimally stimulated in the uninduced cells (Figure 7E). Taken together, these results demonstrate that SOX9 regulates responsiveness to WNT signaling.

WNT-targeted treatment suppresses SOX9-expressing PCa xenograft growth in vivo. To examine the biological significance of WNT signaling in vivo, mice with established VCaP xenografts were randomized to receive treatment with LGK974 or vehicle for 17 days and were then sacrificed. The systemic efficacy of LKG974 in blocking WNT activity was confirmed by reduced *AXIN2* mRNA levels in small intestine crypts, as assessed by ISH (Supplemental Figure 9A). Significantly, tumor growth, as assessed by fold change in tumor volumes, was substantially suppressed by LGK974 (Figure 8A). Consistent with this growth inhibition, BrdU incorporation (mice were pulsed with BrdU prior to sacrifice) in the LGK974-treated xenografts was markedly reduced (Figure 8B). Examination of the xenografts by ISH confirmed that WNT signaling, as assessed by *AXIN2* mRNA, was decreased in the LGK974-treated tumors (Figure 8B and Supplemental Figure 9B).

To further examine the contribution of SOX9-dependent WNT pathway activation in supporting tumor growth, we established xenografts with LNCaP cells expressing a doxycycline-regulated *SOX9* transgene. The level of overexpressed exogenous SOX9 protein in LNCaP xenografts overexpressing SOX9 was comparable to the level of endogenous SOX9 in VCaP xenografts (Supplemental Figure 10). Consistent with our previous report, expression of exogenous SOX9 in LNCaP cells increased the rate at which

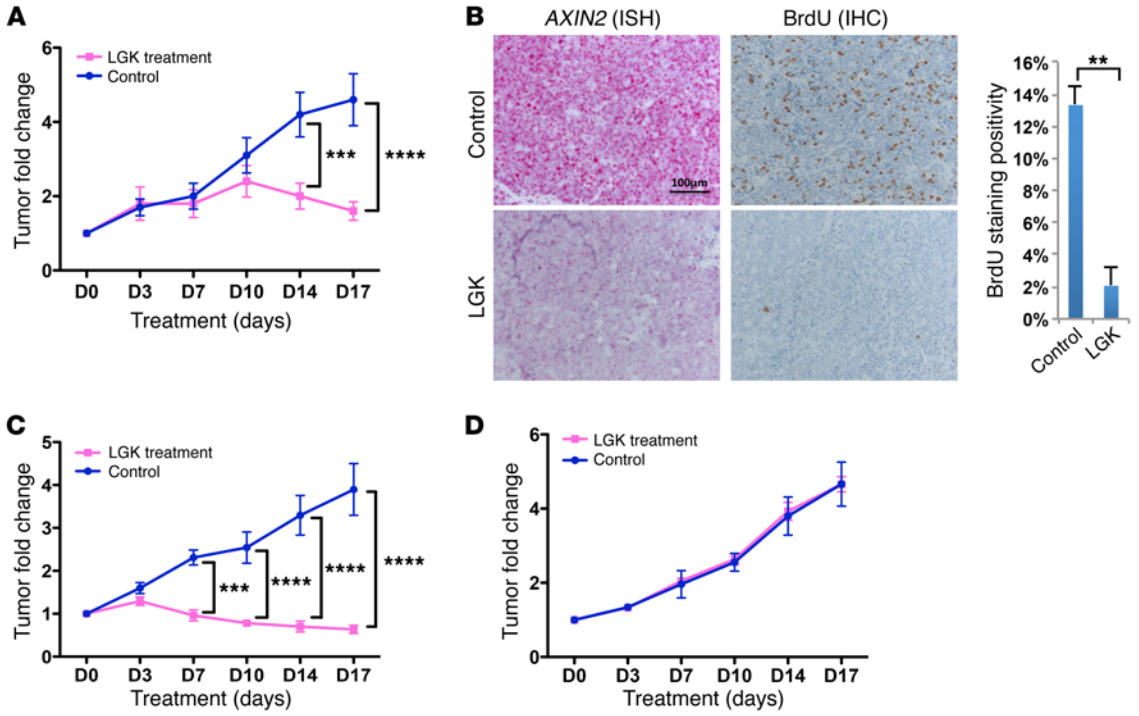

Figure 8. Inhibition of SOX9-dependent WNT activity reduces tumor growth in vivo. (**A**) Mice with established subcutaneous VCaP xenografts were treated daily with i.p. injection of carrier (control, $n = 16$) or of LGK974 (3 mg/kg, $n = 16$). The tumor volume was followed and fold change was calculated by dividing the tumor volume at each time point by its day 0 volume. Two-way ANOVA with Bonferroni post-tests were used to compare replicate means at each time point. ***$P < 0.001$, ****$P < 0.0001$. Error bars represent SEM. (**B**) Representative images of *AXIN2* mRNA ISH in control and LGK974-treated VCaP xenografts. Representative images of BrdU incorporation in control and LGK974-treated VCaP xenografts measured by BrdU IHC. The mean of BrdU incorporation rate was plotted for the control and LGK974-treated groups. Scale bar: 100 mm. Unpaired *t* test was used. **$P < 0.01$. Error bars represent SD. (**C** and **D**) Mice injected with inducible SOX9-overexpressing LNCaP cells were divided into induced (food and water containing doxycycline) or uninduced (fed with regular food and water) groups. Mice with established subcutaneous xenografts from each group were randomly assigned to the control or LGK974 treatment subgroups, and the tumor volumes were followed at described in **A**. (**C**) Tumor growth curve of the control ($n = 8$) and LGK974-treated ($n = 6$) mice in the SOX9-induced group. (**D**) Tumor growth curve of control ($n = 4$) and LGK974-treated ($n = 3$) mice in the uninduced group. Two-way ANOVA with Bonferroni post-tests were used. ***$P < 0.001$, ****$P < 0.0001$. Error bars represent SEM.

xenografts initially developed (data not shown) (13). Mice were treated with doxycycline to induce SOX9 expression at the time of implantation, and those with established tumors were randomized to receive treatment with LGK974 or vehicle (control), as above for the VCaP xenografts. Significantly, the LGK974 treatment arrested tumor growth (Figure 8C). In striking contrast, LGK974 had no effect on the growth of xenografts generated from the same LNCaP cells in the absence of doxycycline induction (Figure 8D) or on xenografts generated from the parental LNCaP cells (Supplemental Figure 11). Significant effects of LGK974, comparable to those shown in Figure 8, were observed when absolute changes in tumor volume were plotted (Supplemental Figure 12), based on fold change in tumor volume. Overall these findings support the conclusion that SOX9 expression enhances tumor cell responsiveness to WNT signaling and that SOX9-mediated WNT pathway activation is critical for the role of SOX9 in promoting tumor growth.

Discussion

WNT signaling plays a key role in many tissues and has been implicated in several cancers. Previous studies have provided evidence of canonical WNT/β-catenin signaling in PCa (47–54), but its role in PCa has been controversial (55). Common mutations observed in colon cancers (such as those in APC, β-catenin, or AXIN1) are infrequent in PCa, and enhanced WNT/β-catenin signaling, as indicated by elevated nuclear β-catenin staining, has been inconsistently found in clinical PCa (56–60). However, it has become clear that nuclear β-catenin staining is not a sensitive indicator of WNT/β-catenin pathway activation and that robust biomarkers and mechanisms of WNT signaling are needed to fully elucidate the role of this pathway in PCa (47–54). We believe that our study establishes a novel link between SOX9 and WNT pathway activation in PCa and shows mechanistically that SOX9 positively regulates multiple genes required for WNT signaling. Significantly, recent studies also support important roles of both SOX9 and canonical WNT/β-catenin signaling in ductal morphogenesis of fetal prostate (10, 11, 34). Based on these findings, we propose that SOX9 expression (driven by *TMPRSS2:ERG* fusion or additional mechanisms) stimulates PCa development by sensitizing cells to WNTs, which may be autocrine and/or from stroma, and thereby reactivates the WNT signaling pathway that regulates ductal morphogenesis in fetal prostate.

While the TCF transcription factors appear to be the major nuclear targets of β-catenin, additional transcription factors may also be coactivated by β-catenin. One such transcription factor is AR, whose interaction with β-catenin may contribute to PCa (61–65). Interestingly, we found that SOX9 directly regulated the

expression of YAP1, which coactivates TEAD transcription factors to turn on genes involved in cell proliferation, survival, and invasion. YAP1 is the major target of the tumor suppressor Hippo pathway, and, in quiescent cells, it undergoes Hippo pathway–mediated serine phosphorylation that inhibits its nuclear import and promotes degradation. Significantly, YAP1 was also recently found to bind β-catenin, with the β-catenin/YAP1 complex coactivating the TBX5 transcription factor and stimulating the expression of prosurvival genes (39). These observations indicate that SOX9 regulates YAP1 transcription directly and may also regulate its activity indirectly through the WNT/β-catenin pathway. Interestingly, and consistent with a recent report (66), using IHC we found that YAP1 in normal prostate is expressed primarily by basal cells, similarly to SOX9. These findings suggest that a physiological function of SOX9 in normal basal cells may be to overcome Hippo and other growth-suppressive pathways by rendering the cells permissive to WNT signals from the stroma that may be produced in response to injury (67).

We reported previously that SOX9 expression was associated with triple-negative breast cancer and that it could stimulate the expression of LRP6 and TCF4 in breast cancer cell lines (37). Moreover, we showed that transgenic overexpression of SOX9 in mammary epithelium caused increased TCF4 expression. A recent study in adult hair follicle stem cells similarly found that SOX9 bound to and regulated the *TCF4* gene, although the effect of SOX9 knockdown on TCF4 and WNT signaling in these cells was modest (26). Our results also indicate that SOX9 directly suppresses the expression of WNT5A, which mediates noncanonical WNT signaling through binding to the ROR1 and ROR2 receptor tyrosine kinases, and suppresses canonical signaling (although this was not observed in LNCaP cells overexpressing SOX9). While our findings indicate that SOX9 sensitizes PCa cells to respond to canonical WNT signaling, SOX9 can bind to and sequester nuclear β-catenin and has been reported to stimulate the phosphorylation and degradation of nuclear β-catenin in chondrocytes (68, 69). This could be a negative feedback mechanism to restrain WNT signaling in normal prostate basal cells, but further studies are needed to determine whether this mechanism plays a role in normal prostate or in prostate carcinogenesis.

Although SOX9 expression may render PCa cells responsive to WNT signals through increased expression of WNT receptors and downstream signaling proteins, these cells may still be dependent on WNT synthesis, which may be autocrine or paracrine from stroma. Our results support the notion that an autocrine WNT synthesis may be activating the pathway in a subgroup of PCa. In addition, stromal WNT production or stromal WNT activation through β-catenin overexpression is sufficient to promote prostate tumorigenesis in mouse models (47, 48, 54). Interestingly, in adult human prostate, stromal WNT16B was identified as a factor mediating epithelial cell resistance to DNA-damaging agents (67). WNT signaling in advanced PCa may also be enhanced by *APC* gene methylation or by mutations in key components of the WNT signaling pathway (70–72). Overall, these findings indicate that WNT synthesis and signaling are driving at least a subset of PCa, in particular those tumors with high SOX9 levels, and that this subset of PCa may be responsive to WNT synthesis inhibitors or other WNT pathway antagonists that are now entering the clinic.

Methods

Cell lines and reagents. Cell lines were from ATCC and were maintained under conditions recommended by the provider. VCaP cells LNCaP cells with doxycycline-regulated SOX9 overexpression (LNCaP-SOX9 cells), and CWR22Rv1 cells with SOX9 silencing shRNA (CWR22Rv1-shSOX9 cells) were previously described (13, 18). WNT inhibitors, LGK974 or PKF118-310, were purchased from ActiveBiochem and Selleckchem, respectively.

RNAi. SOX9 knockdown was as described previously (12). Briefly, cells were transfected with 100 nM siGENOME siRNA (GE Healthcare Dharmacon) using Lipofectamine 2000 (Thermo Fisher Scientific). RNA or protein was extracted at 72 hours after transfection.

RNA isolation and qRT-PCR. Total RNA was isolated using the RNeasy Mini Plus Kit or RNeasy FFPE Kits (Qiagen). qRT-PCR was performed in triplicate using standard SYBR Green reagents from the StepOnePlus Real-Time PCR system (Thermo Fisher Scientific). Target mRNA expression was quantified using the $\Delta\Delta C_t$ method and normalized to *GAPDH* expression. Primer sequences are listed in the Supplemental Methods.

Gene expression arrays. Transcriptome profiling was performed using Affymetrix GeneCHIP Human Genome U133 plus 2.0 Arrays (Affymetrix), all in biological duplicates compared with control. Raw data were analyzed using GeneSpring (Agilent). After ranking according to differential expression, GSEA was performed to search for enrichment across the Molecular Signatures Database (73). GSEA and box plots of SOX9 and its association with WNT components were derived from independent clinical data sets from TCGA and MSKCC (GSE 21032). For SOX9-associated gene expression analysis, two cohorts of patients with PCa were studied (195 patients in the TCGA data set and 131 patients in the MSKCC data set). SOX9 high tumors were defined as those among the top 75% of tumors with positive z scores in the TCGA data set or those among the top 50% in the MSKCC data set. Conversely, SOX9 low tumors were defined as those among the bottom 75% of tumors with negative z scores in the TCGA data set or those among the bottom 50% in the MSKCC data set.

ChIP-seq analysis. ChIP-seq was performed using two independent anti-SOX9 antibodies (Ab1 from Millipore and Ab2 from Abcam). Libraries were sequenced to 50 bps. ChIP-seq reads were aligned to the human genome (NCBI36). Significantly enriched regions ($P < 1 \times 10^{-15}$) were detected with the MACS software using default parameters (74). Genomic features associated with SOX9-binding sites, such as distribution and conservation, were determined using the cis-regulatory element annotation system. The SeqPos motif algorithm in Cistrome was used to define the consensus SOX9-binding motif by compiling the genomic sequences within a 100-bp window centered on the summits of the SOX9 ChIP-seq peaks. In addition, genomic sequences within a 600-bp window centered on the summits of the SOX9 ChIP-seq peaks were scanned for enriched transcriptional factor-binding sites to define the potential SOX9 cofactors. ChIP-seq analysis was performed using Cistrome as previously described (75). The data sets from microarray and ChIP-seq analyses have been deposited in the GEO repository (GSE76452).

Immunoblotting and IHC. Immunoblotting and IHC experiments were performed as described before (12). Briefly, for immunoblotting, proteins were extracted using RIPA buffer. The primary antibodies were incubated overnight. Gels shown are representative of at least 3 independent experiments. Sources and dilutions of the primary anti-

bodies are provided in the Supplemental Methods. For IHC, paraffin sections underwent antigen retrieval and were then incubated with primary antibody overnight at 4°C, followed by biotinylated secondary antibody and streptavidin–horseradish peroxidase (Vector Laboratories). The IHC results were scored blindly of the clinical information. The samples were assigned as low when 0% to 5% of the tumor cells showed positive nuclear staining or assigned as high when more than 25% of the tumor cells showed positive nuclear staining. Sections presented in each figure were stained under same conditions and photographed under identical conditions.

Luciferase reporter assay. Transfections were performed by using X-tremeGENE HP DNA Transfection Reagent (Roche Molecular Biochemicals, Sigma-Aldrich) according to the manufacture's instructions. Briefly, LNCaP SOX9-OE cells were plated in a 96-well plate at a density of 2×10^4 cells per well and were treated with vehicle or doxycycline (100 ng/ml). Twenty-eight hours after seeding, cells were transfected with 100 ng per well of the TOPflash (16× or 8×) or FOPflash (8×) reporter plasmids (Addgene) together with 2 ng per well of a renilla reporter plasmid (pRL-CMV) as a normalization control. Eighteen hours after transfection, WNT3A (40 ng/ml) or vehicle was added to the cells and incubated for an additional 10 hours. Cells were then lysed for 15 minutes at room temperature. The lysates were clarified by centrifugation at 1,900 *g* for 10 minutes, and luciferase reporter gene expression was measured by a Dual-Luciferase Reporter Assay Kit (Promega). The relative firefly luciferase (RFL) activity was obtained by normalizing firefly luciferase activity against renilla luciferase activity. RFL fold change upon WNT3A stimulation was calculated by normalizing the luciferase activity after WNT3A stimulation against the basal activity. All experiments were repeated in triplicate for at least 3 times.

ChIP. Experiments were performed as previously described (18). qPCR (SYBR Green) was used to measure the DNA fragment quantities, which were compared with input DNA to calculate ΔCT values. The relative quantity (RQ) value ($RQ = 2^{-\Delta CT}$) represents the precipitated DNA relative to input. Results are represented as mean ± SD for replicate samples. Data are representative of at least 3 experiments.

RNA ISH. ISH for *SOX9*, *FZD5*, *FZD7*, and *AXIN2* was performed using an RNAscope 2.0 FFPE Assay (Advanced Cell Diagnostics). Briefly, 5-μm sections of FFPE blocks were treated for 1 hour with heat and for a half hour with protease before hybridization with target probes. A horseradish peroxidase–based signal amplification system was then applied and was followed by visualization with DAB. Positive staining was observed as red, punctate dots. Technical controls included the bacterial gene DapB as a negative control and the housekeeping gene PPIB as a positive control. In addition, as a positive control, AXIN2 staining was also validated on a colorectal cancer sample. Each sample was scored blindly of their clinical information or of their SOX9 expression levels. The RNAscope score was scored at a magnification of ×200 or ×400, and the samples were binned into 5 subgroups based on the intensity of positively stained tumor cells. The scoring criteria were as follows: 0, no staining or <3 dots per 10 cells; 1, 1–3 dots per cell; 2, 4–9 dots per cell or no or very few dot clusters; 3, 10–15 dots per cell or <50% dots are in clusters; and 4, >15 dots per cell or >50% dots are in clusters. The score was assigned based on the intensity of the prevalent cell population.

Xenografts and drug treatment. All animal studies were conducted at the Beth Israel Deaconess Medical Center according to protocols approved by their institutional animal care and use committees. VCaP, LNCaP-SOX9, or parental LNCaP xenografts were established in the flanks of 6-weeks-old male SCID or nude mice by injecting approximately 5 million cells in 50% Matrigel. The LNCaP-SOX9 group was feed with doxycycline chow (0.625 g/kg, Harlan Tekland) and water (1 g/l in 1% dextrose), commencing at the initial implantation. Mice bearing established xenografts (tumor volume, 100–200 mm^3) were randomized into control or LGK974 treatment groups, each receiving daily i.p. injections of DMSO or 3 mg/kg LGK974 for 17 days. Tumor sizes were followed twice a week by directly measuring with a caliper. Tumor volumes were calculated with the formula: length × width × width/2. The fold change of tumor volume was determined by normalizing each tumor measurement to its volume on day 0 at the beginning of drug administration. The cell proliferation labeling reagent BrdU was i.p. injected at 24 hours prior to tumor collection, according to the manufacture's instructions (kit RPN201, Amersham, GE Health Care Life Science).

Statistics. Significance of difference between 2 groups was determined by 2-tailed Student's *t* test using Prism5 (GraphPad Software Inc.). For comparison of tumor growth curves between LGK974 treatment and the control, tumor volume fold change data were analyzed by 2-way ANOVA with Bonferroni post-tests to compare replicate means at each measuring time point. Statistical significance was accepted at $P < 0.05$.

Study approval. Mouse xenograft studies were approved by the Beth Israel Deaconess Medical Center IACUC. The analysis of deidentified human tissue samples was approved by the Beth Israel Deaconess Medical Center IRB.

Author contributions

FM, SPB, and XY designed the studies. FM, SJG, SC, BAT, CC, LH, HW, and XY performed various parts of the study. FM, HY, HHH, AGS, SPB, and XY acquired and analyzed the data. FM, SPB, and XY wrote and edited the manuscript.

Acknowledgments

This work was supported by grants from the NIH (R01 DK 079962, R01 CA 168393, P01 CA163227, and P50 CA090381), the Department of Defense Prostate Cancer Research Program (W81XWH-12-1-0158 and W81XWH-15-1-0151), a challenge grant from the Prostate Cancer Foundation, and a grant from the Bridge Project (partnership between the Koch Institute for Integrative Cancer Research at MIT and the Dana-Farber/Harvard Cancer Center). F. Ma was supported by a Millennium Fellowship in Prostate Cancer Research from the American Association of Cancer Research (14-40-38-MA). C. Cai was supported by an NIH Pathway to Independence award (K99 CA166507).

Address correspondence to: Xin Yuan, Division of Hematology/Oncology, Department of Medicine, Beth Israel Deaconess Medical Center, 330 Brookline Ave., CLS-0439, Boston, Massachusetts 02215, USA. Phone: 617.735.2066; E-mail: xyuan@bidmc.harvard.edu. Or to: Steven P. Balk, Division of Hematology/Oncology, Department of Medicine, Beth Israel Deaconess Medical Center, 330 Brookline Ave., CLS-0443, Boston, Massachusetts 02215, USA. Phone: 617.735.2065; E-mail: sbalk@bidmc.harvard.edu.

1. Foster JW, et al. Campomelic dysplasia and autosomal sex reversal caused by mutations in an SRY-related gene. *Nature*. 1994;372(6506):525–530.
2. Wagner T, et al. Autosomal sex reversal and campomelic dysplasia are caused by mutations in and around the SRY-related gene SOX9. *Cell*. 1994;79(6):1111–1120.
3. Blache P, et al. SOX9 is an intestine crypt transcription factor, is regulated by the Wnt pathway, and represses the CDX2 and MUC2 genes. *J Cell Biol*. 2004;166(1):37–47.
4. Lincoln J, Kist R, Scherer G, Yutzey KE. Sox9 is required for precursor cell expansion and extracellular matrix organization during mouse heart valve development. *Dev Biol*. 2007;305(1):120–132.
5. Seymour PA, et al. SOX9 is required for maintenance of the pancreatic progenitor cell pool. *Proc Natl Acad Sci U S A*. 2007;104(6):1865–1870.
6. Vidal VP, et al. Sox9 is essential for outer root sheath differentiation and the formation of the hair stem cell compartment. *Curr Biol*. 2005;15(15):1340–1351.
7. Furuyama K, et al. Continuous cell supply from a Sox9-expressing progenitor zone in adult liver, exocrine pancreas and intestine. *Nat Genet*. 2011;43(1):34–41.
8. Lu B, et al. Analysis of SOX9 expression in colorectal cancer. *Am J Clin Pathol*. 2008;130(6):897–904.
9. Kopp JL, et al. Identification of Sox9-dependent acinar-to-ductal reprogramming as the principal mechanism for initiation of pancreatic ductal adenocarcinoma. *Cancer Cell*. 2012;22(6):737–750.
10. Huang Z, et al. Sox9 is required for prostate development and prostate cancer initiation. *Oncotarget*. 2012;3(6):651–663.
11. Thomsen MK, et al. SOX9 elevation in the prostate promotes proliferation and cooperates with PTEN loss to drive tumor formation. *Cancer Res*. 2010;70(3):979–987.
12. Wang H, McKnight NC, Zhang T, Lu ML, Balk SP, Yuan X. SOX9 is expressed in normal prostate basal cells and regulates androgen receptor expression in prostate cancer cells. *Cancer Res*. 2007;67(2):528–536.
13. Wang H, et al. SOX9 is expressed in human fetal prostate epithelium and enhances prostate cancer invasion. *Cancer Res*. 2008;68(6):1625–1630.
14. Thomsen MK, Butler CM, Shen MM, Swain A. Sox9 is required for prostate development. *Dev Biol*. 2008;316(2):302–311.
15. Schaeffer EM, et al. Androgen-induced programs for prostate epithelial growth and invasion arise in embryogenesis and are reactivated in cancer. *Oncogene*. 2008;27(57):7180–7191.
16. Acevedo VD, et al. Inducible FGFR-1 activation leads to irreversible prostate adenocarcinoma and an epithelial-to-mesenchymal transition. *Cancer Cell*. 2007;12(6):559–571.
17. Zhang X, Cowper-Sal lari R, Bailey SD, Moore JH, Lupien M. Integrative functional genomics identifies an enhancer looping to the SOX9 gene disrupted by the 17q24.3 prostate cancer risk locus. *Genome Res*. 2012;22(8):1437–1446.
18. Cai C, et al. ERG induces androgen receptor-mediated regulation of SOX9 in prostate cancer. *J Clin Invest*. 2013;123(3):1109–1122.
19. Tomlins SA, et al. Role of the TMPRSS2-ERG gene fusion in prostate cancer. *Neoplasia*. 2008;10(2):177–188.
20. Chen Y, et al. ETS factors reprogram the androgen receptor cistrome and prime prostate tumorigenesis in response to PTEN loss. *Nat Med*. 2013;19(8):1023–1029.
21. Yu J, et al. An integrated network of androgen receptor, polycomb, and TMPRSS2-ERG gene fusions in prostate cancer progression. *Cancer Cell*. 2010;17(5):443–454.
22. Huang W, Zhou X, Lefebvre V, de Crombrugghe B. Phosphorylation of SOX9 by cyclic AMP-dependent protein kinase A enhances SOX9's ability to transactivate a Col2a1 chondrocyte-specific enhancer. *Mol Cell Biol*. 2000;20(11):4149–4158.
23. Mertin S, McDowall SG, Harley VR. The DNA-binding specificity of SOX9 and other SOX proteins. *Nucleic Acids Res*. 1999;27(5):1359–1364.
24. Oh CD, et al. Identification of SOX9 interaction sites in the genome of chondrocytes. *PLoS One*. 2010;5(4):e10113.
25. Bhandari RK, Haque MM, Skinner MK. Global genome analysis of the downstream binding targets of testis determining factor SRY and SOX9. *PLoS One*. 2012;7(9):e43380.
26. Kadaja M, et al. SOX9: a stem cell transcriptional regulator of secreted niche signaling factors. *Genes Dev*. 2014;28(4):328–341.
27. Wang G, et al. Zbtb7a suppresses prostate cancer through repression of a Sox9-dependent pathway for cellular senescence bypass and tumor invasion. *Nat Genet*. 2013;45(7):739–746.
28. Taylor BS, et al. Integrative genomic profiling of human prostate cancer. *Cancer Cell*. 2010;18(1):11–22.
29. Haller R, et al. Notch1 signaling regulates chondrogenic lineage determination through Sox9 activation. *Cell Death Differ*. 2012;19(3):461–469.
30. Martini S, et al. A critical role for Sox9 in notch-induced astrogliogenesis and stem cell maintenance. *Stem Cells*. 2013;31(4):741–751.
31. Shih HP, et al. A Notch-dependent molecular circuitry initiates pancreatic endocrine and ductal cell differentiation. *Development*. 2012;139(14):2488–2499.
32. van Leenders GJ, et al. Activation of c-MET induces a stem-like phenotype in human prostate cancer. *PLoS One*. 2011;6(11):e26753.
33. Blache P, et al. SOX9 is an intestine crypt transcription factor, is regulated by the Wnt pathway, and represses the CDX2 and MUC2 genes. *J Cell Biol*. 2004;166(1):37–47.
34. Kruithof-de Julio M, et al. Canonical Wnt signaling regulates Nkx3.1 expression and luminal epithelial differentiation during prostate organogenesis. *Dev Dyn*. 2013;242(10):1160–1171.
35. Gupta S, et al. FZD4 as a mediator of ERG oncogene-induced WNT signaling and epithelial-to-mesenchymal transition in human prostate cancer cells. *Cancer Res*. 2010;70(17):6735–6745.
36. Wu L, Zhao JC, Kim J, Jin HJ, Wang CY, Yu J. ERG is a critical regulator of Wnt/LEF1 signaling in prostate cancer. *Cancer Res*. 2013;73(19):6068–6079.
37. Wang H, et al. SOX9 regulates low density lipoprotein receptor-related protein 6 (LRP6) and T-cell factor 4 (TCF4) expression and Wnt/β-catenin activation in breast cancer. *J Biol Chem*. 2013;288(9):6478–6487.
38. Camargo FD, et al. YAP1 increases organ size and expands undifferentiated progenitor cells. *Curr Biol*. 2007;17(23):2054–2060.
39. Rosenbluh J, et al. beta-Catenin-driven cancers require a YAP1 transcriptional complex for survival and tumorigenesis. *Cell*. 2012;151(7):1457–1473.
40. Minami Y, Oishi I, Endo M, Nishita M. Ror-family receptor tyrosine kinases in noncanonical Wnt signaling: their implications in developmental morphogenesis and human diseases. *Dev Dyn*. 2010;239(1):1–15.
41. Green J, Nusse R, van Amerongen R. The role of Ryk and Ror receptor tyrosine kinases in Wnt signal transduction. *Cold Spring Harb Perspect Biol*. 2013;6(2):a009175.
42. Ho HY, et al. Wnt5a-Ror-Dishevelled signaling constitutes a core developmental pathway that controls tissue morphogenesis. *Proc Natl Acad Sci U S A*. 2012;109(11):4044–4051.
43. Verhaegh W, et al. Selection of personalized patient therapy through the use of knowledge-based computational models that identify tumor-driving signal transduction pathways. *Cancer Res*. 2014;74(11):2936–2945.
44. Liu J, et al. Targeting Wnt-driven cancer through the inhibition of Porcupine by LGK974. *Proc Natl Acad Sci U S A*. 2013;110(50):20224–20229.
45. Lepourcelet M, et al. Small-molecule antagonists of the oncogenic Tcf/beta-catenin protein complex. *Cancer Cell*. 2004;5(1):91–102.
46. Krieghoff E, Behrens J, Mayr B. Nucleo-cytoplasmic distribution of beta-catenin is regulated by retention. *J Cell Sci*. 2006;119(pt 7):1453–1463.
47. Placencio VR, et al. Stromal transforming growth factor-beta signaling mediates prostatic response to androgen ablation by paracrine Wnt activity. *Cancer Res*. 2008;68(12):4709–4718.
48. Li X, et al. Prostate tumor progression is mediated by a paracrine TGF-beta/Wnt3a signaling axis. *Oncogene*. 2008;27(56):7118–7130.
49. Bisson I, Prowse DM. WNT signaling regulates self-renewal and differentiation of prostate cancer cells with stem cell characteristics. *Cell Res*. 2009;19(6):683–697.
50. Pearson HB, Phesse TJ, Clarke AR. K-ras and Wnt signaling synergize to accelerate prostate tumorigenesis in the mouse. *Cancer Res*. 2009;69(1):94–101.
51. Yu X, Wang Y, DeGraff DJ, Wills ML, Matusik RJ. Wnt/beta-catenin activation promotes prostate tumor progression in a mouse model. *Oncogene*. 2011;30(16):1868–1879.
52. Zong Y, et al. Stromal epigenetic dysregulation is sufficient to initiate mouse prostate cancer via paracrine Wnt signaling. *Proc Natl Acad Sci U S A*. 2012;109(50):E3395–E3404.
53. Francis JC, Thomsen MK, Taketo MM, Swain A. β-Catenin is required for prostate development and cooperates with Pten loss to drive invasive carcinoma. *PLoS Genet*. 2013;9(1):e1003180.
54. Carstens JL, et al. FGFR1-WNT-TGF-β signaling in prostate cancer mouse models recapitulates human reactive stroma. *Cancer Res*. 2014;74(2):609–620.
55. Kypta RM, Waxman J. Wnt/β-catenin signalling in prostate cancer. *Nat Rev Urol*. 2012;9(8):418–428.

56. Bismar TA, Humphrey PA, Grignon DJ, Wang HL. Expression of β-catenin in prostatic adenocarcinomas: a comparison with colorectal adenocarcinomas. *Am J Clin Pathol*. 2004;121(4):557–563.
57. de la Taille A, et al. Beta-catenin-related anomalies in apoptosis-resistant and hormone-refractory prostate cancer cells. *Clin Cancer Res*. 2003;9(5):1801–1807.
58. Horvath LG, et al. Lower levels of nuclear β-catenin predict for a poorer prognosis in localized prostate cancer. *Int J Cancer*. 2005;113(3):415–422.
59. Kallakury BV, et al. Decreased expression of catenins (α and β), p120 CTN, and E-cadherin cell adhesion proteins and E-cadherin gene promoter methylation in prostatic adenocarcinomas. *Cancer*. 2001;92(11):2786–2795.
60. Whitaker HC, Girling J, Warren AY, Leung H, Mills IG, Neal DE. Alterations in β-catenin expression and localization in prostate cancer. *Prostate*. 2008;68(11):1196–1205.
61. Truica CI, Byers S, Gelmann EP. β-Catenin affects androgen receptor transcriptional activity and ligand specificity. *Cancer Res*. 2000;60(17):4709–4713.
62. Mulholland DJ, Read JT, Rennie PS, Cox ME, Nelson CC. Functional localization and competition between the androgen receptor and T-cell factor for nuclear β-catenin: a means for inhibition of the Tcf signaling axis. *Oncogene*. 2003;22(36):5602–5613.
63. Yang F, et al. Linking β-catenin to androgen-signaling pathway. *J Biol Chem*. 2002;277(13):11336–11344.
64. Amir AL, Barua M, McKnight NC, Cheng S, Yuan X, Balk SP. A direct β-catenin-independent interaction between androgen receptor and T cell factor 4. *J Biol Chem*. 2003;278(33):30828–30834.
65. Lee E, Madar A, David G, Garabedian MJ, Dasgupta R, Logan SK. Inhibition of androgen receptor and β-catenin activity in prostate cancer. *Proc Natl Acad Sci U S A*. 2013;110(39):15710–15715.
66. Nguyen LT, et al. ERG activates the YAP1 transcriptional program and induces the development of age-related prostate tumors. *Cancer Cell*. 2015;27(6):797–808.
67. Sun Y, et al. Treatment-induced damage to the tumor microenvironment promotes prostate cancer therapy resistance through WNT16B. *Nat Med*. 2012;18(9):1359–1368.
68. Akiyama H, et al. Interactions between Sox9 and β-catenin control chondrocyte differentiation. *Genes Dev*. 2004;18(9):1072–1087.
69. Topol L, Chen W, Song H, Day TF, Yang Y. Sox9 inhibits Wnt signaling by promoting β-catenin phosphorylation in the nucleus. *J Biol Chem*. 2009;284(5):3323–3333.
70. Aryee MJ, et al. DNA methylation alterations exhibit intraindividual stability and interindividual heterogeneity in prostate cancer metastases. *Sci Transl Med*. 2013;5(169):169ra10.
71. Chen Y, et al. APC gene hypermethylation and prostate cancer: a systematic review and meta-analysis. *Eur J Hum Genet*. 2013;21(9):929–935.
72. Robinson D, et al. Integrative clinical genomics of advanced prostate cancer. *Cell*. 2015;161(5):1215–1228.
73. Subramanian A, et al. Gene set enrichment analysis: a knowledge-based approach for interpreting genome-wide expression profiles. *Proc Natl Acad Sci U S A*. 2005;102(43):15545–15550.
74. Zhang Y, et al. Model-based analysis of ChIP-Seq (MACS). *Genome Biol*. 2008;9(9):R137.
75. Liu T, et al. Cistrome: an integrative platform for transcriptional regulation studies. *Genome Biol*. 2011;12(8):R83.